Macromolecules
ARTICLE

Macromolecules **2010**, *43*, 8251–8263 **8251**
DOI: 10.1021/ma101229r

Self-Consistent PRISM Theory−Monte Carlo Simulation Studies of Copolymer Grafted Nanoparticles in a Homopolymer Matrix

Nitish Nair and Arthi Jayaraman*

Department of Chemical and Biological Engineering, University of Colorado UCB 424, Boulder, Colorado 80309

Received June 1, 2010; Revised Manuscript Received August 1, 2010

ABSTRACT: We have used a self-consistent PRISM−Monte Carlo (MC) approach to study copolymer functionalized nanoparticles in a homopolymer matrix and to calculate the potential of mean force (PMF) between the grafted particles (at low grafting density) for varying monomer sequences in the grafted polymer, matrix packing fraction, molecular weight of the grafted and matrix chains, attraction strength between one set of like-monomers, and the nanoparticle diameter. We find that the monomer sequence (alternating and diblock) in the grafted chains dictates how the attractive monomers aggregate and how those aggregates help or hinder matrix-induced direct contacts between the grafted particles, and thus the strength and location of attraction or repulsion in the PMF between two grafted particles. At weak like-monomer attraction strengths ($0.2kT$), the alternating copolymer-grafted particles exhibit a PMF similar to athermal homopolymer-grafted particles. For the diblock copolymer-grafted particles, if the monomers in the block closer to the surface are attractive, the PMF is repulsive at contact and weakly attractive at larger interparticle distances; if the monomers in the outer block are attractive, the PMF is attractive at contact and repulsive at larger interparticle distances. The effect of monomer sequence on the PMF is enhanced by increasing the graft chain length and suppressed by either increasing the matrix packing fraction or using larger nanoparticles. For example, the PMF becomes strongly attractive at contact (a) when the amount of matrix is increased such that the matrix-induced depletion-like attraction between the particles prevails over the steric hindrance from the grafted chains or (b) when the ratio of particle diameter to graft length is increased such that the graft is too short and the grafted monomers can no longer shield the surface from direct interparticle contact. This study demonstrates that grafting copolymers on nanoparticles allows for precise tuning of the magnitude, nature and location of attraction or repulsion in the PMF, which is needed for the tailored assembly of these functionalized nanoparticles in polymer nanocomposites for use in photonics, electronics, and photovoltaic applications.

1. Introduction

Theoretical and experimental work in polymer nanocomposites has established that adding nanoparticles, such as metal particles, carbon nanotubes, and layered silicates, to a polymer matrix enhances the inherent properties of the polymer due to synergistic interactions between the polymer matrix and nanoparticle additives. Conventionally, it is accepted that isotropic dispersion of the nanoparticle additives is essential for improved properties such as reduced permeability, optical clarity, ablation resistance, increased mechanical strength, etc. However, for creating a new generation of spatially engineered polymer nanocomposites that can be used for photonics, solar or photovoltaic (alternative energy), and electronics applications, precise assembly and ordering of nanoparticles mediated by a polymer matrix is extremely important. Highly ordered nanoparticle assemblies in a polymer matrix can be obtained by functionalizing the nanoparticle surface with ligands such as polymers, DNA,[1−8] and proteins[9−11] that can then manipulate the interfacial interactions between the nanoparticles and the matrix the particles are placed in, and thus control their assembly. Past theoretical[12−26] and experimental[27−35] work on *homopolymer*-functionalized nanoparticles has established that the chemistry of the grafted polymers, nanoparticles and the polymer matrix play a critical role in dictating the spatial organization of the nanoparticles. For example, experimental studies[28−30] have achieved the migration of the polymer-grafted nanoparticles from one domain to another domain in the matrix by thermally changing the composition of the grafted homopolymers on the nanoparticle and thus the compatibility of the grafted polymer and matrix. Another important parameter that dictates the effective interparticle interaction, and therefore the particle assembly, is the polymer grafting density, defined as the number of grafted polymers per unit surface area of the nanoparticle. The grafting density and molecular weight dictate the conformations of the grafted polymers. At high grafting density,[19,20,36−39] the grafted polymers extend due to crowding and form a brush-like conformation on the particle surface. Particles carrying a homopolymer brush placed in a homopolymer matrix whose chemistry is identical to the grafted polymer disperse (aggregate) if the molecular weight of the matrix homopolymer is lower (higher) than that of the grafted homopolymer. At low grafting density,[16,22,26,40,41] the grafted polymers do not face any crowding from monomers of adjacent chains and as a result do not stretch into brush-like conformations. The surface of the nanoparticle that is exposed versus that covered by the grafted monomers dictates the effective interparticle interactions.[22−26] Such homopolymer-grafted nanoparticles at low grafting densities have been shown to assemble into a variety of nanostructures in solvent[17,18,42−46] and in polymer matrix.[19,23,24] While most of the above studies establish the effect of various molecular parameters on the behavior of *homopolymer*-grafted nanoparticles either in solvent or in a polymer matrix, the assembly of *copolymer*-grafted nanoparticles in a solvent or

*Corresponding author. E-mail: arthi.jayaraman@colorado.edu.

Published on Web 09/09/2010

polymer matrix has been studied to a much smaller extent.[47−49] Copolymer-grafted nanoparticles have been synthesized successfully; for example, atom transfer radical polymerization (ATRP) has been used to grow random copolymers from the surface of silica nanoparticles,[27] and *Z*-supported reversible addition−fragmentation chain transfer (RAFT) polymerization has been used to synthesize diblock copolymer-grafted silica particles.[50]

In this paper we present a self-consistent polymer reference interaction site model− (PRISM−) Monte Carlo (MC) study of AB copolymer-grafted spherical nanoparticles (at low grafting density) placed in A or B homopolymer matrix. We have studied the effect of monomer sequence (alternating versus diblock) in the grafted chain, molecular weight of the grafted and matrix chains, particle size, matrix packing fraction (dense solutions to melts), and intermonomer attractive strength on the potential of mean force between copolymer-grafted nanoparticles in a homopolymer matrix. This work was motivated by the Monte Carlo simulation study of copolymers of varying monomer sequences grafted onto a single solid spherical nanoparticle,[49] which showed the nontrivial effect of monomer sequence, particle diameter, grafted chain length and grafting density on the grafted copolymer conformations. These parameters dictate if (a) the grafted chains aggregate to bring attractive monomers from multiple grafted chains together (interchain and intrachain monomer aggregation) if the enthalpy gained by doing so offsets the entropic loss caused by the stretching of the chains or (b) each grafted chain folds onto itself to bring the attractive monomers together (purely intrachain monomer aggregation) if the entropic loss from interchain aggregation cannot be overcome by the enthalpic gain but the energetically favorable intrachain contacts compensate for the loss of conformational entropy accompanying the intrachain monomer aggregation. The complex interplay of monomer sequence, grafted chain length, and particle diameter, and their nontrivial effects on the grafted chain conformations, quantified by the radius of gyration and observed through the simulation snapshots, motivates us to study how these parameters affect the potential of mean force between copolymer-grafted nanoparticles placed in a melt-like polymer matrix, and in turn their assembly. Since the possible grafted chain conformations outlined above differ greatly from ideal polymer conformations,[51] we cannot use PRISM theory alone to obtain the potential of mean force as PRISM theory treats the conformations of the chains as constant and ideal. We use a self-consistent approach where the grafted chain conformations that are inputs to PRISM theory are provided by Monte Carlo (MC) simulations of a single copolymer-grafted nanoparticle in an external medium-induced potential obtained from PRISM theory.

Using the self-consistent PRISM−MC approach we observe that alternating and diblock copolymer-grafted particles exhibit significantly different trends in their potentials of mean force (PMF) when we systematically vary the graft chain length, monomer interactions, particle size, and total fluid packing fraction. The monomer sequence dictates how the attractive monomers aggregate and the spatial locations of the attractive monomer aggregates around the nanoparticle surface, while the sizes of the monomer aggregates depend on the intermonomer attraction strength and graft chain length. A combination of these factors dictates the magnitude and nature (attractive or repulsive) of the PMF and the interparticle distance at which the PMF is attractive or repulsive. The effect of monomer sequence on the potential of mean force is increased by increasing the graft chain length and is minimized by either increasing the matrix packing fraction or using nanoparticles of larger diameters. Increased matrix concentration pushes the particles closer leading to an attractive PMF at contact, while increasing the particle size at constant graft chain length and constant grafting density leads to a greater fraction of the particle surface being exposed to direct interparticle contact.

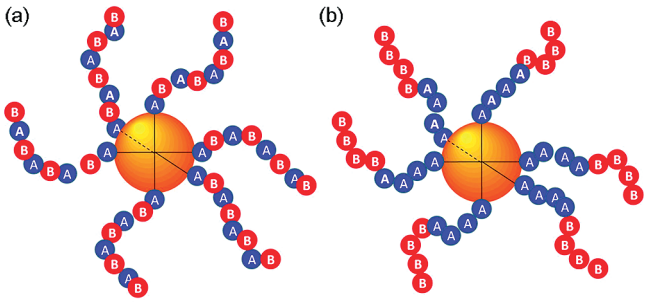

Figure 1. Schematic of copolymer-grafted nanoparticles with (a) alternating monomer sequence and (b) diblock monomer sequence.

The paper is organized as follows. In section 2, we provide details of our model, interaction potentials and the self-consistent PRISM−MC method. In section 3, we present the results showing the effect of varying monomer sequence, packing fraction, grafted chain length, particle diameter and attraction strength on the potential of mean force. We conclude with a discussion on the observed general trends, a critique of the method, and future directions.

2. Model and Methods

2.1. Model and Interactions. We model the system as spherical nanoparticles grafted with six freely jointed AB copolymer chains per particle, placed in a matrix of freely jointed A or B homopolymer chains. The grafted copolymer and matrix homopolymer chains consist of monomer beads of diameter d and bond length $l = 1.4d$ chosen to mimic a Kuhn segment of a linear synthetic polymer. The six grafted copolymers, each consisting of N_g monomers, are permanently attached to the six poles of a hard spherical nanoparticle of diameter D. Each AB copolymer is symmetrically composed of monomeric units—A and B—in either an alternating (Figure 1a) or diblock sequence (Figure 1b). The matrix chains of length N_m have a homopolymer sequence of either A or B. We use the subscripts A, B, C and M to denote the A and B monomers on the grafted chain, the particle, and the monomer on the matrix chain, respectively. The packing fraction, η, is the volume fraction of the system occupied by the matrix chains and the copolymer-grafted nanoparticles (fillers). The volume fraction of η occupied by the copolymer-grafted nanoparticles is denoted by the filler fraction, ϕ. In this paper, we focus only on the infinitely dilute filler limit (or 2 particle limit) and maintain $\phi = 0.001$.

The interactions between nonbonded like-monomers, U_{ii}, in the grafted chain are modeled using the shifted Lennard-Jones (L-J) potential

$$U_{ii}(r) = 4\varepsilon_{ii}\left[\left(\frac{\sigma_{ii}}{r}\right)^{12} - \left(\frac{\sigma_{ii}}{r}\right)^{6} - \left(\frac{\sigma_{ii}}{r_{cut}}\right)^{12} + \left(\frac{\sigma_{ii}}{r_{cut}}\right)^{6}\right] \quad (i = \mathrm{A}, \mathrm{B}) \tag{1}$$

where ε_{ii} is the well-depth; σ_{ii}, the well-width, is the monomer diameter, d; r_{cut} is the cutoff distance beyond which the L-J potential is set to zero. We note that while the Monte Carlo simulation uses the shifted L-J potential with a cutoff of $2.5d$ for computational efficiency, PRISM theory uses the standard L-J potential without any shift or cutoff. In this work we choose only one pair of like grafted monomers (AA or BB) to be attractive and maintain athermal interactions (i.e., hard-sphere potential) between other pairs of like-monomers, all pairs of unlike monomers, particle and particle, and particle and monomer (on grafted and matrix chains).

2.2. Method. PRISM theory consists of a matrix of Ornstein−Zernike-like integral equations that relate the total site−site intermolecular pair correlation function, $h_{ij}(r)$, to the intermolecular

direct correlation function, $c_{ij}(r)$, and intramolecular pair correlation function, $\omega_{ij}(r)$. The PRISM equations as functions of the wavevector q in Fourier space are

$$H(q) = \Omega(q)C(q)[\Omega(q) + H(q)] \quad (2a)$$

$$H_{ij}(q) = \rho_i \rho_j \hat{h}_{ij}(q) \quad (2b)$$

$$\Omega_{ij}(q) = \rho \sum_{\alpha=1}^{N_i} \sum_{\beta=1}^{N_j} \Omega_{\alpha_i \beta_j}(q) \quad (2c)$$

where $H(q)$, $C(q)$, and $\Omega(q)$ in this study are matrices of size 4×4 (for the 4 types of sites A, B, C, and M) with the matrix elements defined in eqs 2b and 2c. In these equations, N_i and ρ_i are respectively the number and number density of site i, ρ is the molecular number density, and $\Omega_{ij}(q)$ the intramolecular pair correlation function in Fourier space between sites i and j within a certain molecule. To solve eqs 2a-c, we use closure relations connecting the real space $c_{ij}(r)$, $h_{ij}(r)$, and interaction potentials, $U_{ij}(r)$. The choice of closures depends on the system being studied; for example, previous work on a mixture of nanoparticles and polymers[23−26,52−57] shows that the Percus−Yevick (PY) closure for polymer−polymer and polymer−particle, and hypernetted chain (HNC) closure for particle−particle work well. We have used the same combination of atomic closures, since this work also consists of polymers and nanoparticles. We note here that molecular closures[58−60] could prove more accurate for copolymer-grafted nanoparticles and their accuracy should be investigated by comparisons with either MC or molecular dynamics simulation results for the same system. We have mentioned this again in section 4 as one of the future directions for improving this method. Given that σ_{ij} is the distance of closest approach between sites i and j, i.e. $\sigma_{ij} = d$ for monomer−monomer pairs and $\sigma_{ij} = D + d/2$ for particle−monomer pairs, the impenetrability condition applies inside the hard core:

$$g_{ij}(r) = 0 \quad r < \sigma_{ij} \quad (3a)$$

Outside the hard core, the PY approximation describes the direct correlation function between all pairs of sites (except particle−particle)

$$c_{ij}(r) = (1 - e^{\beta U_{ij}(r)}) g_{ij}(r) \quad r > \sigma_{ij} \quad (3b)$$

and the HNC closure handles the particle−particle direct correlation function

$$c_{CC}(r) = h_{CC}(r) - \ln g_{CC}(r) - \beta U_{CC}(r) \quad r > D \quad (3c)$$

To efficiently solve this system of coupled nonlinear integral equations we employ the KINSOL algorithm[61] with the line search optimization strategy which minimizes the objective function along an optimum descent direction. Most of the past work using PRISM theory involved solving eqs 2 and 3 using the Picard technique. We have found that KINSOL allows us to attain convergence for complex nonlinear integral equations easier and faster as compared to the Picard technique. The solution of the PRISM equations yields the pair correlation functions, $g_{ij}(r)$, and the partial collective structure factors, $S_{ij}(q)$. We note that some sets of parameters, especially involving higher interaction strengths, do not yield any solutions due to numerical issues.

In *most* past studies of polymer nanocomposites (fillers in homopolymer matrix) using PRISM theory[23−26,52−57] the intramolecular pair correlation, Ω_{ij}, was calculated by assuming *ideal* conformations of the grafted and matrix chains. Since the grafted chains on a copolymer-grafted particle have been shown to form nonideal conformations in simulation studies,[49] using ideal conformations for the graft and matrix chains for this study does not seem valid. Therefore, we use a self-consistent approach linking PRISM theory and Monte Carlo simulations where the chain conformations (or the intramolecular pair correlation function Ω_{ij}) that are inputs to PRISM are provided by MC simulations of a single copolymer-grafted nanoparticle in an external medium-induced potential obtained from PRISM theory. The interdependence of the chain conformations and the medium-induced potential gives rise to the self-consistency. This approach can tackle nonideal conformations along the grafted and matrix polymers that have been neglected in previous studies of homopolymer-grafted nanoparticles.[23−26] Furthermore, in contrast to previous self-consistent PRISM−MC studies on homopolymer melts alone[62−67] or work on bare particles in a homopolymer melt[68,69] where the self-consistent loop involved MC simulations of only one matrix polymer chain, in this study we have used alternate self-consistent loops for a single copolymer-grafted particle and single matrix chain. This ensures that we account for nonidealities *both* in the grafted and in the matrix chain conformations. Our approach is similar to the self-consistent PRISM−MC approach applied to a blend of two polymers where the self-consistent loops involved MC simulations of each polymer.[70,71]

The steps involved in this self-consistent approach are as follows. First, the pairwise decomposed medium-induced solvation potential, $\Delta\psi_{ij}(r)$, is obtained from the PRISM equations and describes the interaction between any two sites i and j as mediated by all the remaining sites in the system, i.e., including the matrix, grafts, and particles themselves. The form of the solvation potential depends on the approximation used in its derivation:[62−64,72−74]

$$\Delta\psi_{ij}^{PY}(r) = -kT \ln[1 + c_{ik}(r) * s_{kk'}(r) * c_{k'j}(r)] \quad (4a)$$

$$\Delta\psi_{ij}^{HNC}(r) = -kT c_{ik}(r) * s_{kk'}(r) * c_{k'j}(r) \quad (4b)$$

$$S(q) = \Omega(q) + H(q) \quad (4c)$$

where "$*$" in eqs 4a and 4b denotes a convolution integral in spatial coordinates; k is the Boltzmann constant and T is the temperature; $S(q)$ in eq 4c is the structure factor in terms of the Fourier transformed intra- and intermolecular pair correlation functions. We have used the PY form between the particle−monomer (AC, BC) and intermonomer (AA, AB, BB, MM) site pairs. We direct the reader to the Supporting Information (Figure S1) where we have shown that the choice of the form of solvation potential (all PY versus all HNC) does not affect our results much. In addition, we have verified our self-consistent algorithm for simpler cases by comparing the predicted radial distribution functions for a homopolymer melt (no filler) with those published by Yethiraj and Hall[67] (Figure S2, Supporting Information) and potentials of mean force between bare particles in a homopolymer melt by Frischknecht et al.[68] (see Figure S3 in the Supporting Information).

The solvation potential, $\Delta\psi_{ij}(r)$, is then fed to the MC simulation of a single copolymer-grafted particle or a single matrix chain. In the MC simulation, the model of the copolymer-grafted particle or the matrix chain is the same as that used in PRISM theory. In the simulation, the total interaction between sites i and j separated by a distance r, $U_{ij}^{tot}(r)$ (i, j = A, B, C, or M), is the sum of $U_{ij}(r)$ and the solvation potential, $\Delta\psi_{ij}(r)$, obtained from the preceding PRISM step. As stated earlier the simulation uses the shifted L-J potential with a cutoff of $2.5d$ for computational efficiency, while PRISM theory uses the standard L-J potential. The effect of this is minimal, with the difference between the U_{ij} profiles from MC and PRISM being negligible at the well-depths used in this paper: $0.0033kT$ at $\varepsilon_{ii} = 0.2kT$ and $0.0164kT$ at $\varepsilon_{ii} = 1kT$.

We alternately simulate (a) a single copolymer-grafted nanoparticle or (b) an isolated matrix chain with the set of solvation

potentials from the most recent iteration of PRISM calculations. In the simulation of a single copolymer-grafted particle, the position of the particle is kept fixed while an ensemble of grafted chain configurations is generated using the continuum configurational bias (CCB) regrowth algorithm[75−79] where the grafted chains are regrown from the second bead onward (the first bead of each grafted chain is permanently grafted to the particle surface). In the simulation of a single matrix chain, the entire matrix chain is regrown. The initialization stage of an MC simulation (single grafted particle or single matrix chain) consists of 1 million MC steps where in 1 MC step N sites along the polymer chain are regrown; $N = N_g - 1$ in the single copolymer-grafted particle simulation and $N = N_m$ in the single matrix chain simulation. The initialization stage is followed by the equilibration stage of 1 million MC steps, where the total energy is averaged over blocks of 10^5 MC steps and equilibrium is said to be achieved when the difference between successive block-averaged energies is less than $0.05kT$ for five consecutive blocks. After equilibrium is achieved, the production stage of 2 million MC steps is started where the block-averaged properties (e.g., energy, radius of gyration etc.) are computed every 5×10^4 MC steps. During the production stage, the intramolecular structure factors between site pairs are sampled every 5×10^4 steps and the ensemble average of the intramolecular structure factors (eqs 5a and 5b) is calculated as follows:

$$\langle \Omega_{XY}(q) \rangle = \frac{1}{N_c N_X} \sum_{i=1}^{N_c} \sum_{j=1}^{N_X} \sum_{l=1}^{N_c} \sum_{m=1}^{N_Y} \left\langle \frac{\sin q|\vec{r}_{j,i} - \vec{r}_{m,l}|}{|\vec{r}_{j,i} - \vec{r}_{m,l}|} \right\rangle \quad (5a)$$

$$\langle \Omega_{XC}(q) \rangle = \frac{1}{1 + N_c N_X} \sum_{i=1}^{N_c} \sum_{j=1}^{N_X} \left\langle \frac{\sin q|\vec{r}_{j,i} - \vec{r}_C|}{|\vec{r}_{j,i} - \vec{r}_C|} \right\rangle \quad (5b)$$

where N_c is the number of chains, X and Y represent sites A and B with N_X and N_Y as the respective number of sites; both N_X and N_Y equal $N_g/2$ for a symmetric copolymer (in simulations of the copolymer-grafted particle). The corresponding Ω denotes either self-correlation ($X = Y$) or cross-correlation ($X \neq Y$); $\vec{r}_{j,i}$ and $\vec{r}_C$ are the position vectors of bead j in chain i, and the center of the nanoparticle, respectively. In the case of MC simulations of a single matrix chain, only eq 5a is required for the intramolecular structure of the matrix chain with $X = Y = M$. The $\langle \Omega(q) \rangle$ obtained from the MC simulations serves as the new input for the following iteration of PRISM calculations.

The self-consistent PRISM−MC iterations are continued until convergence. The convergence criterion is monitored using the sum of squared errors (SSE) of $\Delta\psi_{ij}(r)$ between iterations n and $n + 1$

$$\mathrm{SSE}_{n \to n+1} = \sum_{i,j} \sum_{m=1}^{N_r} [\Delta\psi_{ij}{}^{n+1}(r_m) - \Delta\psi_{ij}{}^{n}(r_m)]^2 \quad (6a)$$

where N_r is the number of points over which real space has been discretized. The subscripts i and j denote those pairs of sites whose interactions are relevant to the MC simulation: AA, AB, AC, BC, BB, and MM. The convergence counter, n, is set to 0 for the first iteration. The *SSE* for the transition $n \to n + 1$ ($n \geq 1$) is expressed relative to that from $0 \to 1$. Convergence is attained when the following criterion is fulfilled three consecutive times:

$$\frac{\mathrm{SSE}_{n \to n+1}}{\mathrm{SSE}_{0 \to 1}} \leq 0.01 \quad (n \geq 1) \quad (6b)$$

2.3. Analysis. At the end of the self-consistent PRISM−MC approach, we obtain the equilibrium intermolecular pair correlation function, $g_{ij}(r) = h_{ij}(r) + 1$, that characterizes the local structure of the grafted nanoparticles and the matrix polymer. The potential of mean force (PMF), $W_{CC}(r)$, is calculated from the particle−particle pair correlation function, $W_{CC}(r) = -kT \ln g_{CC}(r)$.

The ensemble-averaged radius of gyration (R_g) characterizes the conformations of the grafted chains and is dictated by a balance of the chain conformational entropy loss and enthalpic gain from bringing attractive like-monomers together. The radius of gyration is calculated in the MC simulation using

$$\langle R_g{}^2 \rangle = \frac{1}{N_c N_g} \sum_{i=1}^{N_c} \sum_{j=1}^{N_g} (\vec{r}_{j,i} - \vec{r}_{CM,i}) \cdot (\vec{r}_{j,i} - \vec{r}_{CM,i}) \quad (7)$$

where $\vec{r}_{j,i}$ is the position vector of the j^{th} bead and $\vec{r}_{CM,i}$ the location of the center of mass of the i^{th} grafted chain, and N_c is the number of grafted chains. In the case of diblock copolymer grafts, we also calculate $\langle R_g{}^2 \rangle$ for each block in the grafted chain. In this situation, the second summation index, j, runs from 1 to $N_g/2$ for the A block and $N_g/2 + 1$ to N_g for the B block, the averaging term in the denominator becomes $N_c N_g/2$, and $\vec{r}_{CM,i}$ is the position of the center of mass of the chosen block in chain i.

2.4. Parameters Varied. The grafted copolymer chains have A and B monomers arranged in either an (a) alternating sequence (Figure 1a) or (b) diblock sequence (Figure 1b). The interactions between one set of like-monomers on the grafted chain are attractive with the L-J well depth, ε_{ii}, varied between 0 and $1kT$. We have considered two cases for each of those attractive strengths: (a) only A monomers on the grafted chain are attractive, e.g., $\varepsilon_{AA} = 0.2kT$ and all other pairs are athermal; (b) only B monomers on the grafted chain are attractive, e.g., $\varepsilon_{BB} = 0.2kT$ and all other pairs are athermal. To maintain athermal interactions between the matrix chains and grafted chains, when the A monomers in the grafted chains are attractive we assign the matrix to be B homopolymer, and when B monomers on the grafted chain are attractive we assign the matrix to be A homopolymer. The total fluid packing fraction is varied from $\eta = 0.1$ to 0.3; $\eta = 0.1$ represents a dense polymer solution in the matrix, and $\eta = 0.3$ represents a polymer melt. The graft length, N_g, is varied from 12 to 36 and the matrix chain length, N_m, from 12 to 48. Finally, a range of diameters of the nanoparticle—$D/d = 2$, 4, 8—has also been considered.

3. Results

3.1. Alternating versus Diblock Monomer Sequence. In Figure 2, we present the potential of mean force (PMF) between two copolymer-grafted particles ($D/d = 4$, $N_g = 24$) in a homopolymer A or B matrix ($N_m = 24$) at a total fluid packing fraction, η, of 0.1 obtained using the self-consistent PRISM−MC method. Figure 2a is for the alternating sequence and Figure 2b is for the diblock sequence in the grafted chains. We show the PMF at purely athermal conditions where all interactions in the system are treated as hard-sphere potentials (black solid line), and when $\varepsilon_{AA} = 0.2kT$ (circles) and $\varepsilon_{BB} = 0.2kT$ (crosses). At purely athermal conditions, the PMF is identical for alternating and diblock copolymers because the system is effectively a homopolymer-grafted nanoparticle in a homopolymer matrix where the matrix chains are of identical chemistry as the grafted chains. The PMF between athermal homopolymer-grafted nanoparticles is repulsive at contact with a small repulsive peak at short interparticle distances and decreasing repulsion at farther distances. The repulsive PMF is due to the steric repulsion caused by the grafted monomers near the particle surface. The length of the repulsive "tail" in the PMF has been shown to depend mainly on the length of the graft and the matrix packing fraction, with the repulsive tail being longer for longer graft chain length and lower matrix packing fraction.[26]

At a weak attractive monomer−monomer interaction of $0.2kT$, the PMF between the alternating copolymer-grafted particles in a matrix (Figure 2a) for $\varepsilon_{AA} = 0.2kT$ (circles) and

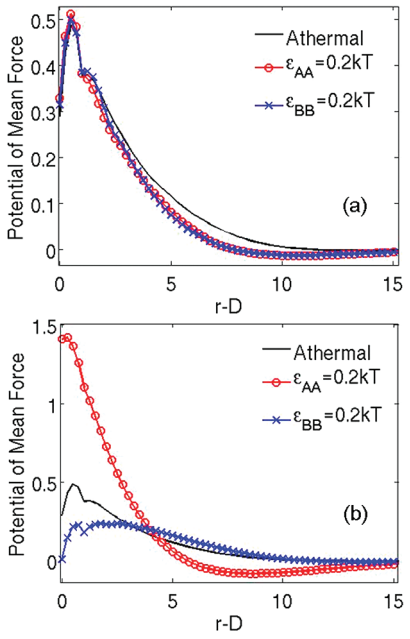

Figure 2. Potential of mean force (in units of kT), $W_{CC}(r)$, as a function of interparticle distance (in units of d), r, between AB copolymer-grafted particles of particle diameter $D/d = 4$ with six grafted copolymers of length $N_g = 24$ having (a) alternating, and (b) diblock sequence in a homopolymer matrix of chain length $N_m = 24$ at packing fraction $\eta = 0.1$. Solid black line represents athermal case, solid red line with circles represents monomer attraction strength $\varepsilon_{AA} = 0.2kT$, and solid blue line with crosses represents $\varepsilon_{BB} = 0.2kT$.

$\varepsilon_{BB} = 0.2kT$ (crosses) is similar to that for the purely athermal PMF. This is unlike the diblock copolymer sequence (Figure 2b) where the PMF between the grafted particles at $\varepsilon_{AA} = 0.2kT$ and $\varepsilon_{BB} = 0.2kT$ differ from the athermal PMF at all $r - D < 15d$ with the deviation at larger interparticle distances being more prominent at $\varepsilon_{AA} = 0.2kT$. The difference in the trends between the alternating and diblock grafted copolymers can be attributed to the differential effect of like-monomer attraction on the grafted chain conformations for alternating and diblock sequences as shown in the simulations of single copolymer-grafted particles.[49] For the alternating copolymer, the conformations at $\varepsilon_{AA} = 0.2kT$ are similar to those adopted at $\varepsilon_{BB} = 0.2kT$ because every A monomer has a B monomer adjacent to it, leading to a frustrated sequence. The conformations that the alternating copolymer adopts with weakly attractive monomers and at purely athermal conditions are similar because the conformational entropic loss of the system upon bringing attractive monomers (when $\varepsilon_{ii} = 0.2kT$) together cannot be overcome by the enthalpy gained from the attractive monomer contacts. This explains why the PMF for the alternating copolymer at $\varepsilon_{AA} = 0.2kT$ and $\varepsilon_{BB} = 0.2kT$ are similar to the athermal PMF. The similar radii of gyration—$3.88d$ for the athermal and $3.81d$ for ε_{AA} or $\varepsilon_{BB} = 0.2kT$—supports this argument that the alternating chains are closer to the athermal than the diblock chains ($R_g \sim 3.77d$) described below.

In contrast to the alternating copolymer sequence, the diblock sequence separates the A and B monomers into two distinct blocks. When $\varepsilon_{AA} = 0.2kT$, the attractive A monomers are conveniently placed next to each other within the A block thus facilitating the attractive A monomers to aggregate. The aggregated A monomers form an A-rich shell on the particle surface since the copolymer chains are grafted on the particle surface by the first bead in the A block (see simulation snapshot in Figure S4a in Supporting Information). The PMF between two grafted particles (circles in Figure 2b) is repulsive at interparticle distances $0 < r - D < 4d$, the region dominated by the A-shell (absent in the athermal case). At $4d < r - D < 14d$, a mild attraction is present due to (a) attractive interactions between the outer layer of the A shells on the two copolymer-grafted particles and (b) because the athermal B monomers do not form an attractive aggregate, and do not hinder the approach of another grafted particle. On the other hand, when $\varepsilon_{BB} = 0.2kT$, the attractive B monomers aggregate far from the particle surface and the athermal A monomers do not aggregate on the particle surface, thus allowing the particle surface to directly contact the surface of another nanoparticle. While the PMF at contact for $\varepsilon_{AA} = 0.2kT$ deviates from the athermal value by $\sim 1kT$, the corresponding difference when $\varepsilon_{BB} = 0.2kT$ is much less ($\sim 0.3kT$) because the matrix monomers are able to screen B monomer attractions in the outer B block much more than the A monomer attractions in the inner A block. At $4d < r - D < 9d$, the PMF is slightly more repulsive for $\varepsilon_{BB} = 0.2kT$ than the PMF at $\varepsilon_{AA} = 0.2kT$ because the attractive B monomers aggregate away from the surface and hinder the approach of another particle. Interestingly, this result is the opposite of what we expected which is that the attractive B monomers from two grafted particles would form contacts and lead to an attractive PMF at that interparticle distance. There are two reasons for this counterintuitive result. First, the attractive monomer strength is not sufficient ($0.2kT$) to bring the grafted particles to the appropriate distance to form intergrafted particle attractive B contacts. Second, it is entropically favorable for the matrix chains to cause depletion-like attraction between the grafted particles that pushes the grafted particles together to contact, as seen in the case of the attractive potential of mean force between bare particles.[52,53,56] In Figure S5a of the Supporting Information, we show that at packing fractions of 0.1, the difference in the PMF at contact between two bare particles and PMF at contact between grafted particles (alternating or diblock sequences) lies in the range $1kT-3kT$ with the bare particles being significantly more likely to aggregate. The matrix-induced depletion-like attraction pushes the particles to contact and the weakly aggregated B monomers hinder this approach, leading to the PMF being repulsive at intermediate distances for $\varepsilon_{BB} = 0.2kT$.

We note here that the *single* grafted particle MC simulation could bias the grafted chain conformations (that are input to PRISM) to consist of monomer contacts *within* a grafted particle and not between grafted particles, which could only slightly deviate from the true behavior of the system if the entropic loss by making intergrafted particle contacts cannot be overcome by the enthalpic gain of those intergrafted particle contacts, e.g. at weak attraction strengths ($\sim 0-0.5$kT). The PRISM calculations allow intergrafted particle contacts so the final self-consistent PRISM−MC solution, the pair correlation function and the potential of mean force, should be minimally affected by these biased conformations input to PRISM. Despite this minor limitation of the self-consistent approach, this self-consistent PRISM−MC approach is better than pure PRISM theory utilizing ideal chain conformations for this system of copolymer-grafted particles because of the nonideal conformations adopted by the grafted chains on the particle. To show how the results from pure ideal PRISM calculations differ from self-consistent PRISM−MC, we present in Figures 3a and 3b the PMF between two grafted particles for the same conditions as in Figure 2a,b but using *ideal* polymer conformations *without* a self-consistent approach. Upon comparing the athermal curves (solid black line in Figures 2a and 3a or Figures 2b and 3b), we observe that the shapes are

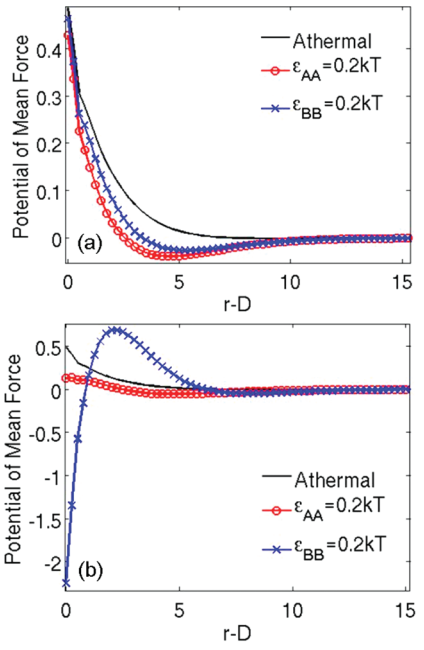

Figure 3. Same as Figure 2. Unlike Figure 2 these results are obtained using pure PRISM calculations with ideal chain conformations.

qualitatively similar (repulsive at contact and at larger r). The differences between the athermal PMF from ideal PRISM and self-consistent approaches are as follows: (i) at contact the self-consistent PMF shows monomer-length scale features which are absent in the ideal PRISM PMF, and (ii) the self-consistent approach has a longer "tail" (Figure 2) than the ideal PRISM calculations (Figure 3). The absence of monomer-length scale features in PRISM calculations using ideal conformations is because intramolecular overlaps are not avoided in PRISM calculations,[67,72] but are avoided in the self-consistent PRISM−MC method through the excluded volume interactions considered in the MC simulation. The presence of a longer repulsive tail in the self-consistent athermal PMF is because the self-consistent treatment of the grafted and matrix chains allows some stretching of the grafted chains not seen in the ideal PRISM calculations. This is confirmed by the R_g for the athermal grafted chains being higher with the self-consistent PRISM−MC approach ($R_g \sim 3.88d$) than the ideal conformations ($R_g \sim (lN_g/6)^{1/2} = 2.37\ d$). Here, it is important to note that past studies of polymer solutions and melts alone[65,70,80] using self-consistent PRISM−MC suggest that the introduction of a $\kappa = 0.9$ prefactor in the HNC solvation potential (eq 4b) is needed at high melt densities to match the chain dimensions from the self-consistent PRISM−MC method to those in MD simulations. Since there are no systematic simulation studies on how the polymer conformations will scale with the addition of fillers (bare or grafted particles) we have used $\kappa = 1.0$ in this work.

For the alternating copolymer, the differences between the PMF obtained from the self-consistent (Figure 2a) and ideal (Figure 3a) approaches at weak monomer attractions are similar to the differences seen between them at athermal conditions. The one additional feature seen for alternating copolymers at $\varepsilon_{AA} = 0.2kT$ and $\varepsilon_{BB} = 0.2kT$ is the presence of a weak midrange attraction in the ideal PMF, which is absent in the corresponding self-consistent PMF. This is explained by the reduced steric hindrance due to intramolecular overlaps in the ideal PRISM calculations; since intramolecular overlaps are avoided in the self-consistent PRISM−MC calculations the PMF does not have the midrange attraction and has a longer repulsive tail as compared to the ideal PRISM PMF.

The diblock copolymer-grafted particles also exhibit the same qualitative differences seen between ideal and self-consistent calculations for the athermal homopolymer, and alternating copolymer at weak attractive interactions. In addition, for the diblock copolymer at $\varepsilon_{AA} = 0.2kT$ the PMF at contact is *less repulsive* for the ideal PRISM calculation (circles in Figure 3b) than self-consistent PRISM (circles in Figure 2b). And, at $\varepsilon_{BB} = 0.2kT$, the PMF at contact is *more attractive* for the ideal PRISM calculation (crosses in Figure 3b) than self-consistent PRISM (crosses in Figure 2b). For $\varepsilon_{BB} = 0.2kT$ in the ideal PRISM calculation there is a repulsive hump of $\sim 0.6kT$ at $r - D \sim 2.5d$ and decays to 0kT around $r - D \sim 6d$, (Figure 3b) while in the corresponding self-consistent calculation the repulsion is weaker and the repulsive tail persists until $r - D \sim 10d$. These results can again be justified by the chains being more stretched in the self-consistent calculations than ideal calculations and by the presence of intramolecular overlaps in the ideal PRISM calculations.

3.2. Varying Matrix Packing Fraction. To describe the effect of packing fraction, we present in Figure 4 the potential of mean force between particles grafted with alternating (Figure 4a) and diblock copolymers (Figure 4b), with $N_g = N_m = 24$ and $D/d = 4$ in the (i) *absence* of a matrix, denoted by $\eta = 0$ for discussion purposes (the actual PRISM calculations reduce to a 3-component A−B−C system with $\eta = 0.0001$), and (ii) *melt-like* matrix ($\eta = 0.3$). The AA or BB interactions are either athermal or mildly attractive with a strength of $0.2kT$.

For alternating copolymer-grafted particles (Figure 4a) the PMF is similar for $\varepsilon_{AA} = 0.2kT$ and $\varepsilon_{BB} = 0.2kT$ at $\eta = 0$ and 0.3, so we have plotted only the $\varepsilon_{AA} = 0.2kT$ curves at $\eta = 0$ and 0.3 in Figure 4a. Furthermore, at both packing fractions, $\eta = 0$ and 0.3, the PMF for the athermal and $\varepsilon_{AA} = 0.2kT$ cases differ negligibly because of the frustrated alternate spacing of A and B monomers along the graft. In the absence of a matrix ($\eta = 0$), the magnitude of repulsion is highest at contact and gradually decays as r increases. The reason for the lack of attraction in the PMF is because (a) the weak attractive interactions between monomers of grafted chains on both particles give them practically no incentive to attract each other (enthalpic gain by doing so does not overcome entropic loss) and (b) due to the absence of the matrix, there are no depletion-like forces pushing the grafted particles together. In the melt-like condition ($\eta = 0.3$), the matrix chains push the grafted particles closer together and induce an attractive PMF of $-2.5kT$ at contact. At $\eta = 0.1$ (in Figure 2a) for the alternating copolymer-grafted particles the PMF at contact is $\sim 0.3kT$, which lies between the corresponding $\eta = 0$ and 0.3 values in Figure 4a. Since the PMF curves are identical for athermal conditions and weak attractive monomer interactions of 0.2kT at $\eta = 0.1$ (Figure 2a), $\eta = 0$, and 0.3 (Figure 4a), we can conclusively say that the attraction at contact between the alternating copolymer-grafted particles is induced purely by the matrix chains, and increasing matrix concentration leads to increasing effective attraction between alternating grafted particles.

The effect of increasing matrix concentration for diblock grafted nanoparticles (Figure 4b and Figure 2b) is similar to the athermal homopolymer and alternating grafted nanoparticles discussed above. As the amount of matrix increases the PMF goes from repulsive to attractive at contact and there is a higher degree of monomer-length scale ordering at $\eta = 0.3$ marked by the peaks and valleys in the PMF, which

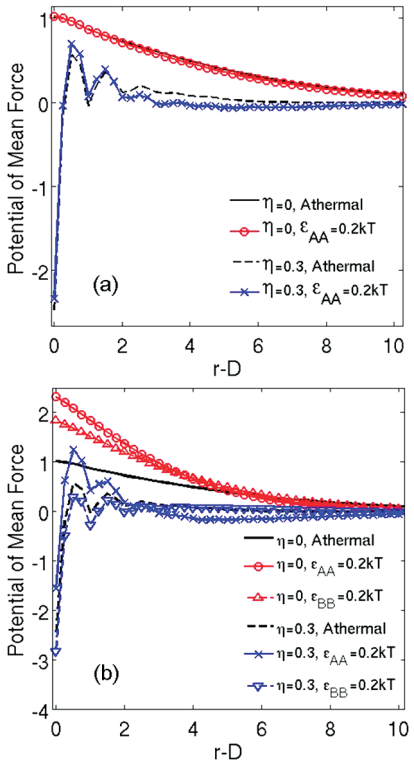

Figure 4. Potential of mean force (in units of kT), $W_{CC}(r)$, as a function of interparticle distance (in units of d), r, between AB copolymer-grafted particles of diameter $D/d = 4$, six grafted copolymers of length $N_g = 24$ with (a) alternating, and (b) diblock sequence, in the absence of matrix ($\eta = 0$) and in a homopolymer matrix of chain length $N_m = 24$ at total packing fractions $\eta = 0.3$, the attraction strengths varying from athermal, $\varepsilon_{AA} = 0.2kT$, and $\varepsilon_{BB} = 0.2kT$.

is seen only marginally in the dense solution case ($\eta = 0.1$). In Figure S5b of the Supporting Information, we show the difference in the PMF at contact between two bare particles and PMF at contact between grafted particles (alternating or diblock sequences) at packing fractions of 0.3; although the bare particles are significantly more likely to aggregate than grafted particles as seen at $\eta = 0.1$ the higher matrix concentration at $\eta = 0.3$ causes the PMF of bare and grafted particles to be similar qualitatively.

The one interesting feature seen for diblock copolymer-grafted particles in the absence of matrix ($\eta = 0$), is that the repulsion at contact for both $\varepsilon_{AA} = 0.2kT$ (circles in Figure 4b) and $\varepsilon_{BB} = 0.2kT$ (up-triangles in Figure 4b) exceeds the repulsion at contact under athermal conditions (solid black line in Figure 4b), in contrast to the alternating grafted particles where the difference in PMF between athermal and attractive interactions was minimal. The magnitude of repulsion between two diblock copolymer-grafted particles is greater when $\varepsilon_{AA} = 0.2kT$ than when $\varepsilon_{BB} = 0.2kT$. This is because unlike the alternating case, in the diblock copolymer the weakly attractive A monomers form a shell on the particle surface that cannot make attractive contacts with the A monomers on the other grafted particle because matrix-induced depletion-like forces that push these grafted particles together are absent at $\eta = 0$, leading to a repulsive PMF at $r - D = 0$; Similarly, the weakly attractive B monomers only form weak intragrafted particle contacts away from the particle surface. Hence, if there is no matrix present, completely athermal grafts provide lower steric hindrance than when either ε_{AA} or $\varepsilon_{BB} = 0.2kT$ because of the lack of intrachain aggregates in case of the purely athermal grafts.

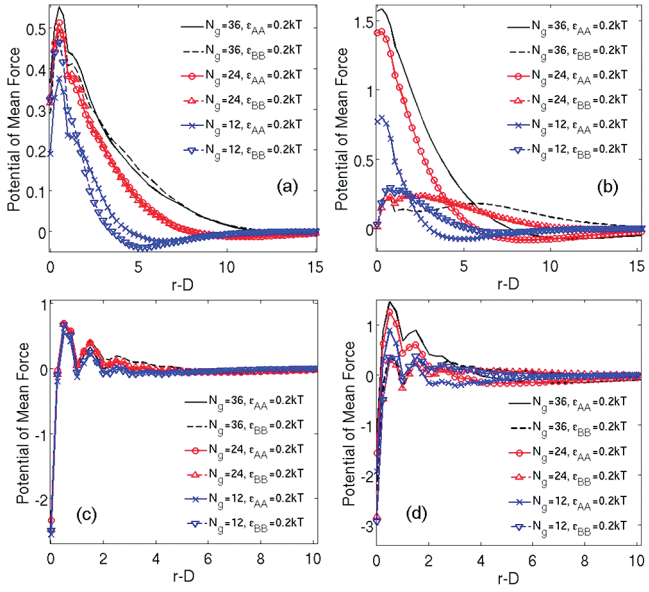

Figure 5. Potential of mean force (in units of kT), $W_{CC}(r)$, as a function of interparticle distance (in units of d), r, between AB copolymer-grafted particles of diameter $D/d = 4$, six grafted copolymers with alternating (a, c), and diblock (b, d) sequence in a homopolymer matrix with chain length $N_m = 24$ at packing fraction $\eta = 0.1$ (a, b) and $\eta = 0.3$ (c, d). The grafted chain length is varied as $N_g = 36$ (black lines), $N_g = 24$ (red lines), and $N_g = 12$ (blue lines).

3.3. Varying Grafted Chain and Matrix Chain Length. To study the effect of the length (or molecular weight) of the grafted and matrix chains on the PMF, we present in Figure 5 the PMF between two copolymer-grafted particles ($D/d = 4$) with alternating and diblock sequences with *varying grafted chain lengths* ($N_g = 12$, 24 and 36) placed in a homopolymer matrix ($N_m = 24$) with a total fluid packing fraction of 0.1 (top row) and 0.3 (bottom row).

At $\eta = 0.1$, for alternating grafted particles (Figure 5a) at all N_g considered here, the PMF at $\varepsilon_{AA} = 0.2kT$ and $\varepsilon_{BB} = 0.2kT$ are similar; the PMF for both cases remain repulsive and have approximately the same magnitude ($0.2-0.3kT$) at contact indicating that the vicinity of the particle surface for direct particle contact is equally inaccessible for all N_g. At $r - D \sim 5d$, there is a weak midrange attraction only for $N_g = 12$; this could be because the graft is too short (and has a frustrated alternating sequence) to make any energetically favorable intragrafted particle attractive contacts, and instead makes a few attractive contacts with the monomers on the other grafted particle facilitated by the reduced steric hindrance because of shorter graft length. An increase in N_g leads to longer repulsive tails in the PMF because long grafts extend farther into the matrix than short ones, hindering the matrix-induced attraction between the particles. The radii of gyration of the alternating copolymer grafts for $N_g = 12$, 24, and 36 are $2.45d$, $3.81d$, and $4.93d$ respectively.

At $\eta = 0.1$ for the diblock copolymer-grafted particles (Figure 5b), as N_g increases the difference in the PMF between $\varepsilon_{AA} = 0.2kT$ and $\varepsilon_{BB} = 0.2kT$ increases. At $\varepsilon_{AA} = 0.2kT$, as N_g increases the PMF at contact becomes more repulsive and the repulsive tail becomes longer. This is because at higher N_g more attractive A monomers envelope the particle surface (thicker A-shell), leading to stronger repulsion at contact and at small r. At $N_g = 12$, there is a weak midrange attraction at $r - D \sim 5d$, similar to the alternating copolymer, due to the reasons discussed above. As N_g increases the repulsive tail in the PMF extends to larger r, due to the larger A block pushing the athermal B block to dangle further away

from the particle. At $\varepsilon_{BB} = 0.2kT$ for the diblock copolymer-grafted particles, the PMF at contact stays the same at all N_g while the weak repulsive hump in the PMF is pushed further away from the particle surface as N_g increases from 12 to 36 because the aggregates of weakly attractive B monomers are pushed to larger r by the larger athermal A block.

At increased packing fraction, $\eta = 0.3$ (Figure 5, parts c and d), the matrix-induced attraction between the two grafted nanoparticles dominates for both alternating and diblock copolymer-grafted particles. Furthermore, the effect of the monomer-sequence on the PMF is also diminished, as is evident from the qualitative similarity in the PMF in Figure 5c (alternating) and Figure 5d (diblock). For both sequences the higher matrix concentration eliminates any effect of graft length on the PMF because the depletion-like attraction between the grafted particles induced by matrix chains dominates the physics of the system; this is evident in the lower R_g of the grafted alternating chains at $\eta = 0.3$: $R_g = 2.27d$, $3.4d$, and $4.32d$ for $N_g = 12$, 24, and 36, respectively, compared to the corresponding values at $\eta = 0.1$.The increased push of the matrix chains yields a highly attractive PMF at contact: $-2.5kT$ at $\eta = 0.3$ versus a repulsive PMF ($+0.3kT$) at $\eta = 0.1$. The peaks at higher r in the PMF are due to higher monomer-level ordering of the nanoparticles caused by the increased number of matrix chains. For the diblock grafted particle (Figure 5d) at $\varepsilon_{AA} = 0.2kT$, the PMF at contact is attractive ($-2kT$) for $\eta = 0.3$ in contrast to the repulsive PMF at contact ($> +0.5kT$) for $\eta = 0.1$; the magnitude of the PMF is almost independent of the length of the A-block or alternatively the thickness of the shell formed by the attractive A monomers. This implies that the increased matrix-induced attraction between the particles at $\eta = 0.3$ is able to overcome the repulsion due to the protective A-shells. This effect of increased matrix-induced attraction is also seen at $\varepsilon_{BB} = 0.2kT$ where we observe a more attractive PMF at contact ($-3kT$) for $\eta = 0.3$ than the corresponding $\eta = 0.1$ case ($0-0.1kT$).

So far we have maintained the matrix chain length constant and varied graft chain length. Past work on homopolymer-grafted particles at *high grafting density*[19,22] has shown that the *relative* length of the grafted and matrix chains is key to the potential of mean force being repulsive (the matrix chain wets the grafted brush layer when $N_m < N_g$) or attractive (the matrix chain dewets the grafted brush layer when $N_m > N_g$). We do not expect brush physics to hold for our system because of the low density of grafted chains on the particles in this paper ($=6$ chains/$\pi D^2 \sim 0.1$ chains/nm^2 for $D/d = 4$). To test this, we present in Figure 6 the PMF between two copolymer-grafted particles ($D/d = 4$) with $N_g = 24$ placed in a homopolymer *matrix of varying lengths*—$N_m = 12$, 24, and 48—at a total fluid packing fraction of 0.1 (top row) and 0.3 (bottom row) for alternating and diblock copolymers. For both graft sequences, the differences in the PMF between various N_m are minimal ($< 0.2kT$) at $\eta = 0.1$ (Figure 6a,b), and even lower at $\eta = 0.3$ (Figure 6c,d). If wetting (dewetting) by the matrix chains had taken place, we would have seen greater repulsion (attraction) between the grafted particles for $N_m < N_g$ ($N_m > N_g$) as compared to the $N_g = N_m$ case. For all the variations, $N_m > N_g$, $N_m = N_g$ and $N_m < N_g$, the average R_g of the grafted chains has been estimated as $3.82d$ (alternating) and $3.77d$ (diblock).

3.4. Varying Particle Size. In Figure 7, we present the potential of mean force between two copolymer-grafted particles of *varying particle diameters* ($D/d = 2$, 4 and 8) with grafted chain length $N_g = 24$ placed in a homopolymer matrix of length $N_m = 24$ at a total fluid packing fraction of

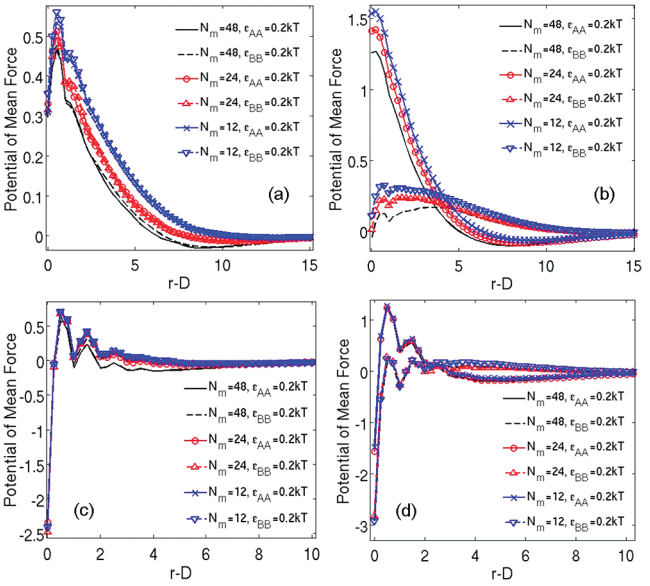

Figure 6. Potential of mean force (in units of kT), $W_{CC}(r)$, as a function of interparticle distance (in units of d), r, between AB copolymer-grafted particles of diameter $D/d = 4$, six grafted copolymers of length $N_g = 24$ with alternating (a, c), and diblock (b, d) sequence in a homopolymer matrix at packing fraction $\eta = 0.1$ (a, b) and $\eta = 0.3$ (c, d). Matrix chain length is varied as $N_m = 48$ (black lines), $N_m = 24$ (red lines), and $N_m = 12$ (blue lines).

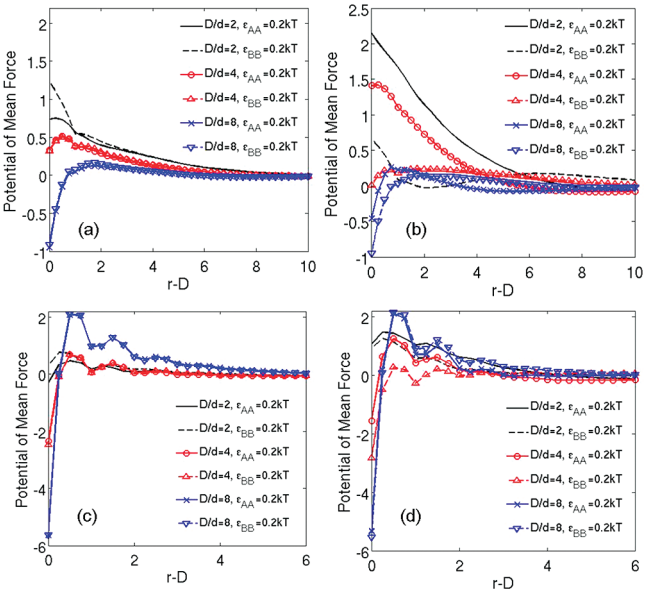

Figure 7. Potential of mean force (in units of kT), $W_{CC}(r)$, as a function of interparticle distance (in units of d), r, between AB copolymer-grafted particles, six grafted copolymers of length $N_g = 24$ with alternating (a, c), and diblock (b, d) sequences in a homopolymer matrix with chain length $N_m = N_g$ at packing fraction $\eta = 0.1$ (a, b) and $\eta = 0.3$ (c, d). The particle diameter is varied as $D/d = 2$ (black lines), 4 (red lines), and 8 (blue lines).

0.1 (top row) and 0.3 (bottom row) for alternating and diblock copolymers, respectively.

At $\eta = 0.1$ in the case of the alternating copolymer (Figure 7a), as the particle size increases from $D/d = 2$ to $D/d = 4$, the PMF at contact decreases in repulsion, and at $D/d = 8$, it is attractive ($-1kT$). This behavior is similar to homopolymer-grafted nanoparticles under athermal conditions (see Figure S6 in the Supporting Information), where an increase in particle diameter for constant grafted chain

length leads to an attractive PMF at contact. Past work[26] using ideal PRISM calculations for homopolymer-grafted nanoparticles also showed similar behavior under athermal conditions; at constant grafted chain length, the PMF at contact changed from repulsive to attractive as the particle size increased because at low grafting densities the extent of exposed particle surface that allows for direct particle contacts governs the PMF. When the particle size is small enough for all the grafted monomers to shield the surface of one particle from another, the PMF at contact is repulsive due to the steric hindrance of the grafted monomers resisting the matrix-induced push at nonmelt packing fractions. When the particle size is too large for all the monomers to shield the surface, the exposed particle offers no resistance to matrix-induced direct contact with another particle surface and the PMF is attractive at contact. As D/d increases from 2 to 8, the difference in PMF at contact between $\varepsilon_{AA} = 0.2kT$ and $\varepsilon_{BB} = 0.2kT$ decreases, the highest difference being $\sim 0.5kT$ for $D/d = 2$. This difference of ~0.5kT between the PMF at contact for $\varepsilon_{AA} = 0.2kT$ and PMF at contact for $\varepsilon_{BB} = 0.2kT$ for D/$d = 2$ is intriguing because we do not expect the weak like-monomer attractive interactions to affect the PMF between grafted particles for the alternating sequence. A more thorough investigation revealed that the bond length, $l = 1.4d$, becomes an important parameter as the particle diameter decreases and becomes comparable. The PMF at contact for $\varepsilon_{AA} = 0.2kT$ and $\varepsilon_{BB} = 0.2kT$ differ negligibly when the grafted chains are composed of tangential beads, i.e., $l = d$ (Figure S7 in the Supporting Information). The polymer chain is clearly longer when $l = 1.4d$, which enables it to seek like-monomers in neighboring grafts (interchain monomer aggregation) within the grafted particle. At $D/d = 2$, the particle diameter is small enough to permit such interchain contacts within the same copolymer-grafted nanoparticle. The number of such attractive interchain contacts is greater when B monomers are attractive than when A monomers are attractive because the six grafted A beads are permanently bonded to the particle surface, restraining them from contributing significantly to the overall A contacts.

At $\eta = 0.1$ in the case of diblock copolymers (Figure 7b), the effect of varying particle size on the PMF is not the same for $\varepsilon_{AA} = 0.2kT$ and $\varepsilon_{BB} = 0.2kT$. When $\varepsilon_{AA} = 0.2kT$ the PMF at contact becomes more repulsive as D/d decreases, similar to the athermal homopolymers (Figure S6 in Supporting Information) and alternating copolymers but the PMF at contact for $D/d = 2$, 4, and 8 are more repulsive by $0.5-1kT$ than the corresponding athermal grafts because of the presence of the shell of A monomers on the surface. When $\varepsilon_{BB} = 0.2kT$ the PMF at contact for each D/d is less repulsive than the corresponding $\varepsilon_{AA} = 0.2kT$ case although the magnitude of the difference at contact decreases with the particle diameter: $1.5kT$, $1.4kT$, and $0.5kT$ for $D/d = 2$, 4 and 8, respectively. As the particle diameter increases at constant graft length, the exposed surface area increases allowing direct particle contacts for all sequences. Thus, the effect of monomer sequence decreases with increasing D. This is evident in the similarity between the PMF plots for the alternating and diblock grafted particles with $D/d = 8$ (Figure 7a,b).

Parts c and d of Figure 7 depict the results for the same parameters as those in Figure parts a and b of 7 but at $\eta = 0.3$. For alternating grafted particles (Figure 7c) at both ε_{AA} and $\varepsilon_{BB} = 0.2kT$, the PMF becomes increasingly attractive at contact as D/d increases from 2 to 8, and peaks close to the particle surface indicative of monomer-level ordering grow more intense as D/d increases from 4 to 8. The higher matrix concentration pushes the particles closer together forcing a tighter monomer layer around the particle surface. This is reflected in the lower radius of gyration of the grafted chains at higher η: for $D/d = 4$, $R_g = 3.81d$ ($\eta = 0.1$) and $3.41d$ ($\eta = 0.3$), and for $D/d = 8$, $R_g = 3.76d$ ($\eta = 0.1$) and $3.36d$ ($\eta = 0.3$).

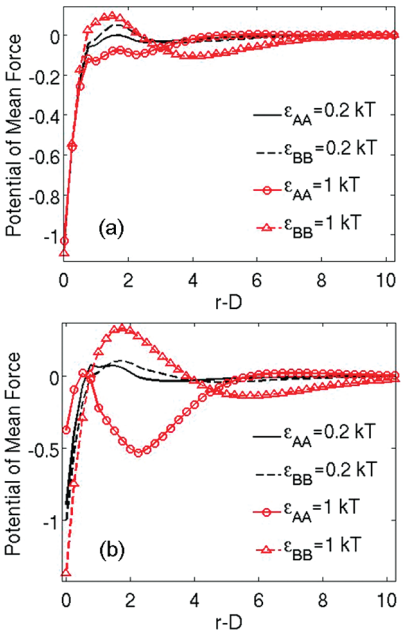

Figure 8. Potential of mean force (in units of kT), $W_{CC}(r)$, as a function of interparticle distance (in units of d), r, between AB copolymer-grafted particles of diameter $D/d = 8$, six grafted diblock copolymers of length (a) $N_g = 8$ and (b) $N_g = 12$ in a homopolymer matrix with chain length $N_m = N_g$ at packing fraction $\eta = 0.1$. The like-monomer attraction strength is varied as $\varepsilon_{ii} = 0.2kT$ and $\varepsilon_{ii} = 1kT$.

For diblock grafted particles at $\eta = 0.3$ (Figure 7d), the PMF at contact is attractive due to increased matrix-induced attraction between the grafted particles, with the exception of $D/d = 2$ where the particle size is small compared to the graft length so that the grafted chains are able to resist matrix-induced attraction leading to a repulsive PMF at contact. At all D/d, the nature of attractive monomer interactions, i.e., either AA or BB, and the consequent aggregation of A or B monomers, respectively, determine the shapes of the PMF profiles. As D/d increases the difference between the PMF curves for $\varepsilon_{AA} = 0.2kT$ and $\varepsilon_{BB} = 0.2kT$ gradually diminishes. The similarity between the PMF for the alternating and diblock grafted particles at $D/d = 8$ (Figure 7a,b and Figure 7c,d) shows that the monomer sequence plays an insignificant role for large nanoparticles.

3.5. Varying Monomer Attraction Strength. Finally, we explore the effect of higher monomer attraction strength (ε_{AA}, $\varepsilon_{BB} = 1kT$) on the PMF of *diblock* grafted particles. We do not present alternating copolymer results because as we approached higher monomer−monomer attraction strengths, the PRISM equations could not converge to a solution due to numerical issues arising in the complex system of nonlinear PRISM equations. This was also true for diblock copolymers for certain sets of parameters. We present in Figure 8, one set of results for which we were able to get converged solutions. Figure 8 shows the potentials of mean force between *diblock* copolymer-grafted particles as ε_{ii} increases from $0.2kT$ to $1kT$ with $D/d = 8$, $N_g = N_m = 8$ (Figure 8a) and $N_g = N_m = 12$ (Figure 8b) at $\eta = 0.1$.

In Figure 8a, the weak attractive strength ($0.2kT$) coupled with the short grafted chain length ($N_g = 8$) and large particle size ($D/d = 8$) leads to an attractive PMF both for $\varepsilon_{AA} = 0.2$kT and $\varepsilon_{BB} = 0.2$kT. This is because the particle surface is easily accessible, since the attractive A-shell or

B-rich "blobs" formed by the diblock grafts are too small compared to the large particle diameter to sterically hinder direct interparticle contacts. When ε_{ii} increases from $0.2kT$ to $1kT$, the PMF at contact remains attractive ($-1kT$) irrespective of whether the A or B beads are attractive because the particle surface continues to be easily accessible for direct interparticle contact induced by the matrix chains. But beyond contact the PMFs for ε_{AA} and ε_{BB} differ for the higher strength of attraction. When $\varepsilon_{AA} = 1kT$, the PMF at $d < r - D < 3d$ is weakly attractive because the graft is too short for intragrafted particle aggregates to be formed so there is intergrafted particle attractive monomer aggregation. When $\varepsilon_{BB} = 1kT$, the PMF is repulsive at $d < r - D < 3d$ due to the steric hindrance caused by the athermal A monomers, and the PMF is attractive for $3d < r - D < 7d$ because the attractive B monomers on both particles aggregate together readily in contrast to the absence of the intergrafted particle aggregates observed at the lower attraction strength of $0.2kT$. The midrange attraction in the PMF is due to the significant enthalpic gain coming from the intergrafted particle contacts at the stronger monomer attraction strength of $1kT$ than at $0.2kT$.

For the longer graft and matrix length $N_g = N_m = 12$ (Figure 8b), the PMF for both ε_{AA} and $\varepsilon_{BB} = 0.2kT$ are similar to the corresponding curves for $N_g = N_m = 8$ (Figure 8a) because the particle size is large enough ($D/d = 8$) and the attraction weak enough that the increase of the graft and matrix lengths by 4 monomers is insignificant. When $\varepsilon_{AA} = 1kT$ the stronger A attractions promote the formation of a tight A-shell (R_g of A block = $1.56d$ at $\varepsilon_{AA} = 0.2kT$ and $1.4d$ at $\varepsilon_{AA} = 1kT$), causing the PMF at contact to be *less* attractive for $\varepsilon_{AA} = 1kT$ than the $\varepsilon_{AA} = 0.2kT$ case. The attractive dip in the PMF for $d \le r - D \le 5d$ corresponds to the attractive contacts between the A monomers of the two copolymer-grafted nanoparticles. When $\varepsilon_{BB} = 1kT$, we see attraction at contact, a repulsive peak at $d \le r - D \le 4d$ and a weak attractive well at $4d \le r - D \le 10d$ in Figure 8b. One would expect that like-monomer attraction strength of 1kT between B monomers would lead to enthapically favorable intergrafted particle contacts and thus a deeper attractive well at intermediate interparticle distances in the PMF. As stated earlier the *single* grafted particle MC simulation could be biasing the grafted chain conformations (that are input to PRISM) to consist of monomer contacts *within* a grafted particle and not monomer contacts between grafted particles. Although the PRISM calculation involves two grafted particles in an explicit polymer matrix, and allows intergrafted particle contacts mediated by the explicit matrix chains, the final self-consistent PRISM−MC-derived PMF could be affected by these biased conformations input to PRISM. To what extent these biased conformations affect the PMF depends on the system parameters. This is discussed in detail in the next section under the critique of this method.

4. Discussion

We have developed a self-consistent PRISM−Monte Carlo (MC) approach directed toward the study of copolymer-grafted nanoparticles placed in a homopolymer matrix. The following parameters have been varied in this study: monomer sequence in the grafted chain (alternating and diblock), matrix packing fraction (η), length of grafted (N_g) and matrix chains (N_m), attraction strength between one pair of like-monomers (ε_{AA} or ε_{BB}) and the nanoparticle diameter (D). We have studied the effect of these parameters on the potential of mean force between copolymer-grafted particles in a homopolymer matrix.

4.1. General Trends for Copolymer-Grafted Particles in Homopolymer Matrix. The motivation behind this work was to prove that varying the monomer sequence in copolymer-grafted nanoparticles allows for the precise tuning of effective interactions between grafted particles in a polymer matrix and thus the morphology in the resulting polymer nanocomposite. To this end, we have studied alternating and diblock grafted particles in a homopolymer matrix, and focused on the effect of monomer sequence and the other parameters listed above on the potential of mean force between the grafted particles. A recurring theme in the results is that the potential of mean force between two alternating grafted particles is insensitive to the type of like-monomer attraction (AA or BB) regardless of the other system parameters, if the like-monomer attraction strength is weak (~0.2−1kT). In dense solutions of polymer matrix and weak like-monomer attractions (ε_{AA} or $\varepsilon_{BB} = 0.2kT$), the behavior of the alternating grafted particles is identical to the behavior of particles with athermal homopolymer grafts. The weak attraction strength coupled with the frustrated −ABAB− monomer arrangement does not permit the alternating grafted chain to assume a compact structure or have intergrafted particle contacts, since the subsequent conformational entropic loss is not overcome by a significant enthalpic gain. As a result of this inherent structural frustration, the grafts assume a configuration that is similar to the athermal case. In contrast, the diblock grafted particles exhibit a richer set of trends even for weak like-monomer attraction strengths. The formation of aggregates of blocks of A or B monomers and how they aid or hinder the matrix-induced attractive interactions between the particles dictate the magnitude, nature and location of attraction/repulsion in the potential of mean force between two grafted particles. The block of attractive A monomers being closer to the particle surface forms a protective shell that hinders matrix-induced direct contact with another particle. The block of attractive B monomers forms aggregates away from the nanoparticle surface and the athermal A monomers do not form a shell on the surface thus leading to matrix-induced attraction at contact and B-aggregate-induced steric repulsion at larger interparticle distances. Higher matrix packing fractions reduce the dependence of the PMF on the monomer sequence and intermonomer attractions because matrix-induced depletion-like forces exerted on the grafted particles dominate and overcome the steric hindrance caused by the conformations of the grafts, and push the grafted particles closer together.

In this study we have focused on six copolymer chains grafted on a particle of diameter varying from ~2 to 8 nm, therefore working at a medium-low grafting density. The effective interactions between *densely* grafted particles in a polymer matrix, where the matrix chain and graft chain have identical chemistry, have been shown[19−22,34,35,38] to depend on the relative lengths of the grafted and matrix chains. In this study for copolymer-grafted particles at *low grafting densit*y, at constant graft length (N_g), when the matrix chain length (N_m) is varied ($N_m < N_g$, $N_m = N_g$, $N_m > N_g$), the PMF at contact differs only by $0.1-0.2kT$ for both alternating and diblock grafts, while maintaining the same quality (i.e., repulsion or attraction) at constant packing fraction. At constant matrix length ($N_m = 24$), when the graft length is varied, for alternating grafts the PMF at contact stayed the same (within $0.2kT$) for all N_g and the PMF beyond contact (repulsive tail) depended on how far the grafted chain extended into the matrix. For diblock grafts, when A monomers are attractive the thickness of the A-shell, which is directly proportional to $N_g/2$, dictates the repulsive PMF at contact; when the B monomers were attractive, the PMF at contact was similar for all graft lengths.

Past work on homopolymer-grafted nanoparticles at low grafting density[22,25,26] suggests that the fraction of nanoparticle surface area exposed dictates the strength of the attractive PMF at contact. This paper has further demonstrated that the monomer sequence and intermonomer attraction strength control the amount of particle surface exposed. In addition, at constant graft length, as particle size D/d increases we observed: (a) a greater portion of the particle surface is exposed to the surroundings unobstructed by the grafted chains; (b) the role of monomer sequence gradually vanishes as evidenced by the similar PMF plots for the alternating and diblock grafted particles at larger particle sizes; (c) type of like-monomer attractions—AA or BB—affect the PMF to a smaller extent, since the difference between the respective PMF values at contact for the diblock grafts decreases, for example from $1.5kT$ ($D/d = 2$) to $0.5kT$ ($D/d = 8$) at $\eta = 0.1$.

We have shown that for diblock grafts weak like-monomer attractive strengths ($0.2kT$) can produce distinguishing characteristics between the PMF when A monomers are attractive and the PMF when B monomers are attractive. For instance, the formation of a distinct A shell next to the surface when $\varepsilon_{AA} = 0.2kT$ or the formation of B aggregates away from the surface when $\varepsilon_{BB} = 0.2kT$ yields a difference in the PMF at contact and at larger interparticle distances, respectively. An increase in the intermonomer attraction strength ($0.2kT$ versus $1kT$) has a minor effect on the PMF for large particles and short graft chain lengths because of the small number of attractive units within the grafted chain; furthermore, whether the A or B monomers are attractive has little effect on the PMF at short graft lengths. As the graft length increases an attraction strength of $1kT$ is potent enough to appreciably alter the behavior of the diblock grafted particles depending on which block is attractive. We expect longer grafts ($N_g = 24, 36$, etc.) to further exploit the differences between AA and BB attractions, but could not prove this due to the difficulty in convergence of the PRISM equations to a solution, one of the limitations of this method discussed further in the next section.

This analysis of copolymer-grafted nanoparticles in a homopolymer matrix using self-consistent PRISM−MC serves as a guide for future experiments by scanning a large parameter space and identifying a subset that most influences the behavior of the system. For instance, the properties of diblock grafted particles are worth studying—in contrast to their alternating counterparts—from the perspective of creating nanoparticle arrays with different periodicities depending on the strength of AA or BB attractions within the diblock chain and the length of the grafted chain itself. The PRISM−MC method can also estimate the matrix concentration above which the matrix chains simply cause the nanoparticles to aggregate thereby nullifying the other system parameters. Particle aggregation can also occur when the grafting density is sparse; this may be prevented by customizing the graft length to the particle diameter and tuning the monomer−monomer and monomer−particle interactions suitably. Experiments may therefore be tailored to study the most sensitive variables after an initial theoretical assessment by the PRISM−MC technique.

4.2. Critique of the Self-Consistent PRISM−MC Approach. The self-consistent PRISM−MC approach used in this work involves obtaining one of the inputs to PRISM—the conformations of the various components of the system—from the MC simulation of a single grafted particle and MC simulation of a single matrix chain in an external medium-induced potential obtained from PRISM theory. This self-consistent approach enables us to avoid the assumption that the chain conformations remain ideal as done in most past applications of PRISM theory to polymer nanocomposites.[23−26,52−54,56] We have observed significant differences in the potential of mean force between particles grafted with alternating or diblock chains, obtained from ideal and self-consistent calculations (comparing Figures 2 and 3), especially at low η. As η increases to melt-like conditions, the self-consistent and ideal results begin to coincide, which is expected because the ideal intramolecular structures of the polymer chains are reasonably accurate under these dense conditions. As stated in the results section, one of the limitations of the self-consistent PRISM−MC approach is that the *single* grafted particle MC simulation could be biasing the grafted chain conformations (that are input to PRISM) to consist of monomer contacts *within* a grafted particle and not monomer contacts *between* grafted particles. Although the PRISM calculation involves two grafted particles in an explicit polymer matrix, and allows intergrafted particle contacts mediated by the explicit matrix chains, the final PMF derived from self-consistent PRISM−MC could be affected by these biased conformations input to PRISM. To what extent these biased conformations make the predicted PMF deviate from the true PMF depends on the system parameters. The choice of system parameters dictates the complex interplay of the enthalpy and entropy of the system and eventually whether intragrafted particle contacts or intergrafted particle contacts are favorable. If the system parameters favor intragrafted particle contacts, the results from our self-consistent PRISM approach should not be affected by the MC simulations biasing the grafted chain conformations to consist of intragrafted particle contacts.

How does this self-consistent PRISM−MC approach compare to those from pure MC simulations in an *implicit* matrix and *explicit* matrix? In MC simulations of grafted particles in an *implicit* matrix any spatial arrangements that could be occurring due to excluded volume interactions with matrix chains are ignored; in contrast these excluded volume interactions are taken into account by the PRISM component in the self-consistent PRISM−MC approach. If we compare our approach to the MC simulation of grafted particles in an *explicit* melt-like matrix, the results are obtained much faster with the PRISM−MC approach. However, it is important to evaluate how closely the self-consistent PRISM−MC results will match those obtained from simulations of copolymer-grafted nanoparticles in an *explicit melt-like* homopolymer matrix. Currently, there are no MC simulations or molecular dynamics (MD) simulations of copolymer-grafted nanoparticles at such low grafting densities in an explicit dense polymer matrix available for comparison, partly due to the computational intensity of the simulations at such melt-like densities. We note that the most recent work by Smith and co-workers presenting MD simulations of the potential of mean force between two homopolymer-grafted nanoparticles in a polymer matrix is for *densely* grafted nanoparticles (0.4 and 0.8 chains/nm^2 versus 0.1 chains/nm^2 in our system)[22]. Perhaps the best way to answer the question posed above is by reviewing how past work on self-consistent PRISM−MC studies of polymer melts (no fillers) compared to corresponding results from simulations. The earliest implementations of self-consistent PRISM−MC[62,63] did not obtain the intramolecular structure, Ω, directly from MC as we have done for grafted particles or as others have performed for single polymer chains.[64−66] Instead, the mean end-end distance of the polymer chain, $\langle R^2 \rangle$, was computed from MC and the corresponding Ω was calculated from a semiflexible chain model.[81] Even so, a comparison of the final $\langle R^2 \rangle$ with MC simulations of tangent hard-sphere chains[67] matched within 10% at different chain

lengths and dense packing fractions.[63] It was also noted that *quantitative* comparisons with simulation data were possible at low densities.[62] Khalatur and Khokhlov[64] reported agreement between self-consistent PRISM−MC predictions and MD simulations for a single polymer freely jointed chain in explicit solvent when the HNC-type closure and HNC-derived solvation potentials were used. Putz et al.[66] found a qualitative agreement in the total structure factor for polyolefins modeled in a united atom framework with corresponding MD data. For a system comprising polymer chains and individual solvent sites, Mendez et al.[65] obtained good agreement in the intermolecular solvent−solvent and solvent−polymer pair correlation functions between PRISM and MD simulations. Recently, Frischknecht and co-workers[68] have extended the self-consistent PRISM−MC approach to studying bare spherical particles in a homopolymer matrix. Higher volume fractions of these nanoparticles in the polymer matrix were found to perturb the matrix chain dimensions by increasing the radius of gyration. These findings were commensurate with neutron scattering results, indicating the qualitative accuracy of self-consistent PRISM−MC approach. While the above studies are significant, the system we have studied in this paper is far more complex due to the presence of both grafted chains on the particle and matrix chains. Also, despite simulating the copolymer-grafted particle and matrix chain with the most recent list of solvation potentials, the copolymer-grafted particle and the matrix chain are not explicitly coupled to each other. And as stated earlier, the conformations of the grafted chains could be biased toward a single grafted particle system because the single molecule MC simulation does not *explicitly* include other grafted particles. Therefore, we expect that these self-consistent PRISM results for this complex system of copolymer-grafted nanoparticles in polymer matrix will not quantitatively match the corresponding results from simulations of grafted particles in an explicit polymer matrix. Instead, this approach provides a quick *qualitative* assessment of a large parameter space and identifies key parameters that can then be focused on in experiments of these polymer nanocomposites with polymer-grafted particles as fillers.

The predictions resulting from this self-consistent PRISM−MC approach can be improved in accuracy using further in-depth studies of each system on a case-by-case basis. Some of the planned future directions are as follows. First, for copolymer-grafted particles in a homopolymer matrix we have used atomic PY and HNC closures;[58,59,82] the adoption of molecular closures[58−60] in future work should increase the accuracy of the calculations. Second, we need to evaluate how to rescale the conformations of the polymer chains and as a result the prefactor in the solvation potential equation, as has been done for polymer melts without fillers. This requires explicit MD or MC simulations of the polymer-grafted particles in a polymer matrix, a computationally intensive task, and a direction we are working toward. Third, we plan to extend this study to finite concentrations of polymer-grafted particles (fillers) in a polymer matrix. For a finite filler concentration, we need to establish an improved self-consistent loop by providing to PRISM the conformations obtained from MC simulation of *multiple* polymer-grafted particles in implicit matrix using a PRISM-calculated solvation potential that only has the effective interactions due to the matrix chains. By using an MC simulation of multiple grafted particles in an *implicit* matrix in the self-consistent PRISM−MC loop, we will remove any bias toward intragrafted particle contacts which we currently have due to the MC simulation of a single molecule. Finally, we need to investigate numerical algorithms used for solving the PRISM equations to overcome the numerical convergence issues we face for certain parameters, e.g., longer polymer lengths or higher monomer attraction strengths.

Acknowledgment. This work was partially supported by the National Science Foundation under Grant Number CBET-0930940 and partially by University of Colorado new faculty funds. The authors thank Dr. A. Frischknecht for useful discussions.

Supporting Information Available: Additional data (Figures S1−S9) including the effect of the solvation potential expression, comparison of the PMF between bare particles and grafted particles in a homopolymer matrix, the effect of nonideality in the self-consistent PRISM−MC calculations on the potential of mean force between the grafted particles. This material is available free of charge via the Internet at http://pubs.acs.org.

References and Notes

(1) Park, S. Y.; Lytton-Jean, K. R. A.; Lee, B.; Weigand, S.; Schatz, G. C.; Mirkin, C. A. *Nature* **2008**, *451*, 553–556.
(2) Biancaniello, P. L.; Kim, A. J.; Crocker, J. C. *Phys. Rev. Lett.* **2005**, *94*, 058302.
(3) Lukatsky, D. B.; Mulder, B. M.; Frenkel, D. *J. Phys.: Condens. Matter* **2006**, *18*, S567–S580.
(4) Harris, N. C.; Kiang, C. H. *Phys. Rev. Lett.* **2005**, *95*, 046101–4.
(5) Lazarides, A. A.; Schatz, G. C. *J. Phys. Chem. B* **2000**, *104*, 460–467.
(6) Tkachenko, A. V. *Phys. Rev. Lett.* **2002**, *89*, 148303.
(7) Talanquer, V. *J. Chem. Phys.* **2006**, *125*, 194701.
(8) Parak, W. J.; Pellegrino, T.; Micheel, C. M.; Gerion, D.; Williams, S. C.; Alivisatos, A. P. *Nano Lett.* **2003**, *3*, 33–36.
(9) Stevens, M. M.; Flynn, N. T.; Wang, C.; Tirrell, D. A.; Langer, R. *Adv. Mater.* **2004**, *16*, 915–918.
(10) Slocik, J. M.; Tam, F.; Halas, N. J.; Naik, R. R. *Nano Lett.* **2007**, *7*, 1054–1058.
(11) Si, S.; Mandal, T. K. *Langmuir* **2007**, *23*, 190–195.
(12) Witten, T. A.; Pincus, P. A. *Macromolecules* **1986**, *19*, 2509–2513.
(13) Laub, C. F.; Koberstein, J. T. *Macromolecules* **1994**, *27*, 5016–5023.
(14) Kim, J. U.; Matsen, M. W. *Macromolecules* **2008**, *41*, 4435–4443.
(15) Himmi, M.; Benhamou, M.; Bettachy, A.; Daoud, M. *J. Mol. Liq.* **2003**, *102* (1−3), 347–363.
(16) Marla, K. T.; Meredith, J. C. *J. Chem. Theory Comput.* **2006**, *2*, 1624–1631.
(17) Iacovella, C. R.; Horsch, M. A.; Zhang, Z.; Glotzer, S. C. *Langmuir* **2005**, *21*, 9488–9494.
(18) Horsch, M. A.; Zhang, Z.; Glotzer, S. C. *Nano Lett.* **2006**, *6*, 2406–2413.
(19) Akcora, P.; Liu, H.; Kumar, S. K.; J., M.; Li, Y.; Benicewicz, B. C.; Schadler, L. S.; Acehan, D.; Panagiotopoulos, A. Z.; Pryamitsyn, V.; Ganesan, V.; Ilavsky, J.; Thiyagarajan, P.; Colby, R. H.; Douglas, J. F. *Nat. Mater.* **2009**, *8*, 354–359.
(20) Harton, S. E.; Kumar, S. K. *J. Polym. Sci., Part B: Polym. Phys.* **2008**, *46*, 351–358.
(21) Pryamtisyn, V.; Ganesan, V.; Panagiotopoulos, A. Z.; Liu, H. J.; Kumar, S. K. *J. Chem. Phys.* **2009**, *131*, 221102.
(22) Smith, G. D.; Bedrov, D. *Langmuir* **2009**, *25*, 11239–11243.
(23) Jayaraman, A.; Schweizer, K. S. *Langmuir* **2008**, *24*, 11119–11130.
(24) Jayaraman, A.; Schweizer, K. S. *J. Chem. Phys.* **2008**, *128*, 164904.
(25) Jayaraman, A.; Schweizer, K. S. *Macromolecules* **2008**, *41*, 9430–9438.
(26) Jayaraman, A.; Schweizer, K. S. *Macromolecules* **2009**, *42*, 8423–8434.
(27) Goel, V.; Chatterjee, T.; Bombalski, L.; Yurekli, K.; Matyjaszewski, K.; Krishnamoorti, R. *J. Polym. Sci., Part B: Polym. Phys.* **2006**, *44*, 2014–2023.
(28) Chiu, J. J.; Kim, B. J.; Kramer, E. J.; Pine, D. J. *J. Am. Chem. Soc.* **2005**, *127*, 5036–5037.
(29) Kim, B. J.; Fredrickson, G. H.; Kramer, E. J. *Macromolecules* **2008**, *41*, 436–447.
(30) Costanzo, P. J.; Beyer, F. L. *Macromolecules* **2007**, *40*, 3996–4001.
(31) Causin, V.; Yang, B. X.; Marega, C.; Goh, S. H.; Marigo, A. *J. Nanosci. Nanotechnol.* **2008**, *8*, 1790–1796.
(32) Tsubokawa, N. *Polym. J.* **2007**, *39*, 983–1000.
(33) Li, C.; Han, J.; Ryu, C. Y.; Benicewicz, B. C. *Macromolecules* **2006**, *39*, 3175–3183.

(34) Xu, C.; Ohno, K.; Ladmiral, V.; Composto, R. J. *Polymer* **2008**, *49*, 3568–3577.
(35) Xu, J.; Qiu, F.; Zhang, H.; Yang, Y. *J. Polym. Sci., Part B: Polym. Phys*. **2006**, *44*, 2811–2820.
(36) Corbierre, M. K.; Cameron, N. S.; Sutton, M.; Laaziri, K.; Lennox, R. B. *Langmuir* **2005**, *21*, 6063–6072.
(37) Kim, B. J.; Bang, J.; Hawker, C. J.; Kramer, E. J. *Macromolecules* **2006**, *39* (12), 4108–4114.
(38) Lan, Q.; Francis, L. F.; Bates, F. S. *J. Polym. Sci., Part B: Polym. Phys*. **2007**, *45*, 2284–2299.
(39) Shull, K. R. *J. Chem. Phys*. **1991**, *94*, 5723–5738.
(40) Lee, J. Y.; Balazs, A. C.; Thompson, R. B.; Hill, R. M. *Macromolecules* **2004**, *37*, 3536–3539.
(41) Striolo, A. *Small* **2007**, *3*, 628–635.
(42) Chan, E. R.; Zhang, X.; Lee, C. Y.; Neurock, M.; Glotzer, S. C. *Macromolecules* **2005**, *38*, 6168–6180.
(43) Glotzer, S. C.; Horsch, M. A.; Iacovella, C. R.; Zhang, Z. L.; Chan, E. R.; Zhang, X. *Curr. Opin. Colloid Interface Sci*. **2005**, *10* (5−6), 287–295.
(44) Iacovella, C. R.; Keys, A. S.; Horsch, M. A.; Glotzer, S. C. *Phys. Rev. E*. **2007**, *75*, 040801.
(45) Zhang, Z.; Horsch, M. A.; Lamm, M. H.; Glotzer, S. C. *Nano Lett*. **2003**, *3*, 1341–1346.
(46) Zhang, X.; Chan, E. R.; Glotzer, S. C. *J. Chem. Phys*. **2005**, *123*, 184718.
(47) Chantawansri, T. L.; Bosse, A. W.; Hexemer, A.; D., C. H.; Garcia-Cervera, C. J.; Kramer, E. J.; Fredrickson, G. H. *Phys. Rev. E* **2007**, *75*, 031802.
(48) Kim, J. U.; Matsen, M. W. *Phys. Rev. Lett*. **2009**, *102*, 078303.
(49) Seifpour, A.; Spicer, P.; Nair, N.; Jayaraman, A. *J. Chem. Phys*. **2010**, *132*, 164901.
(50) Zhao, Y. L.; Perrier, S. *Macromolecules* **2006**, *39*, 8603–8608.
(51) Rubinstein, M.; Colby, R. H. *Polymer Physics*; Oxford University Press: Oxford, U.K., 2008.
(52) Hooper, J. B.; Schweizer, K. S. *Macromolecules* **2005**, *38*, 8858–8869.
(53) Hooper, J. B.; Schweizer, K. S. *Macromolecules* **2006**, *39*, 5133–5142.
(54) Hooper, J. B.; Schweizer, K. S.; Desai, T. G.; Koshy, R.; Keblinski, P. *J. Chem. Phys*. **2004**, *121*, 6986–6997.
(55) Hall, L. M.; Anderson, B. J.; Zukoski, C. F.; Shweizer, K. S. *Macromolecules* **2009**, *42*, 8435–8442.
(56) Hall, L. M.; Schweizer, K. S. *J. Chem. Phys*. **2008**, *128*, 234901.
(57) Hall, L. M.; Schweizer, K. S. *Soft Matter* **2010**, *6*, 1015–1025.
(58) Schweizer, K. S. *Macromolecules* **1993**, *26*, 6033–6049.
(59) Schweizer, K. S.; Yethiraj, A. *J. Chem. Phys*. **1993**, *98*, 9053–9079.
(60) Yethiraj, A.; Schweizer, K. S. *J. Chem. Phys*. **1993**, *98*, 9080–9093.
(61) Hindmarsh, A. C.; Brown, P. N.; Grant, K. E.; Lee, S. L.; Serban, R.; Shumaker, D. E.; Woodward, C. S. *ACM Trans. Math. Software* **2005**, *31* (3), 363–396.
(62) Grayce, C. J.; Yethiraj, A.; Schweizer, K. S. *J. Chem. Phys*. **1994**, *100*, 6857–6872.
(63) Melenkevitz, J.; Schweizer, K. S.; Curro, J. G. *Macromolecules* **1993**, *26*, 6190–6196.
(64) Khalatur, P. G.; Khokhlov, A. R. *Mol. Phys*. **1998**, *93*, 555–572.
(65) Mendez, S.; Curro, J. G.; Putz, M.; Bedrov, D.; Smith, G. D. *J. Chem. Phys*. **2001**, *115*, 5669–5678.
(66) Putz, M.; Curro, J. G.; Grest, G. S. *J. Chem. Phys*. **2001**, *114*, 2847–2860.
(67) Yethiraj, A.; Hall, C. K. *J. Chem. Phys*. **1991**, *96*, 797–807.
(68) Frischknecht, A. L.; McGarrity, E. S.; Mackay, M. E. *J. Chem. Phys*. **2010**, *132*, 204901.
(69) Khalatur, P. G.; Zherenkova, L. V.; Khokhlov, A. R. *Eur. Phys. J. B* **1998**, *5*, 881–897.
(70) Heine, D. R.; Grest, G. S.; Curro, J. G. *Adv. Comput. Simul. Approaches Soft Matter Sci. I* **2005**, *173*, 209–249.
(71) Heine, D.; Wu, D. T.; Curro, J. G.; Grest, G. S. *J. Chem. Phys*. **2003**, *118*, 914–924.
(72) Schweizer, K. S.; Curro, J. G. *Macromolecules* **1988**, *21*, 3070–3081.
(73) Grayce, C. J.; Schweizer, K. S. *J. Chem. Phys*. **1994**, *100*, 6846–6856.
(74) Schweizer, K. S.; Curro, J. G. *Adv. Polym. Sci*. **1994**, *116*, 319–377.
(75) de Pablo, J. J.; Laso, M.; Suter, U. W. *J. Chem. Phys*. **1991**, *96*, 2395–2403.
(76) de Pablo, J. J.; Laso, M.; Suter, U. W. *J. Chem. Phys*. **1992**, *96*, 6157–6162.
(77) Siepmann, J. I. *Mol. Phys*. **1990**, *70*, 1145–1158.
(78) Siepmann, J. I.; Frenkel, D. *Mol. Phys*. **1992**, *75*, 59–70.
(79) Frenkel, D.; Smit, B., *Understanding Molecular Simulations: From Algorithms to Applications*. Academic Press: San Diego, CA, 2001.
(80) Mendez, S.; Curro, J. G. *Macromolecules* **2004**, *37*, 1980–1986.
(81) Honnell, K. G.; Curro, J. G.; Schweizer, K. S. *Macromolecules* **1990**, *23*, 3496–3505.
(82) Yethiraj, A.; Schweizer, K. S. *J. Chem. Phys*. **1992**, *97*, 1455–1464.